Graphitic carbon nitride based photocatalysis for redox conversion of arsenic(III) and chromium(VI) in acid aqueous solution

Zhao Wang[a], Muthu Murugananthan[b], Yanrong Zhang[a],*

[a] Environmental Science Research Institute, Huazhong University of Science and Technology, Wuhan 430074, PR China
[b] Department of Chemistry, PSG College of Technology, Peelamedu, Coimbatore 641004, India

ARTICLE INFO

ABSTRACT

In this study, the synergistic redox conversion of As(III) and Cr(VI) in acidic media was efficiently achieved with a graphitic carbon nitride (g-C$_3$N$_4$) based photocatalyst material (with pyromellitic diimide doping) under visible light irradiation. The non-adsorptive nature of As(V) on the g-C$_3$N$_4$ based photocatalyst made it very steady in recycle treatment of both pollutants compared to traditional titanium dioxide based photocatalysts (P25). While the adsorption of few Cr(III) on the photocatalyst would activated photogenerated hydrogen peroxide (H$_2$O$_2$) to yield hydroxyl radical. The As(III)/Cr(VI) conversion was effective at initial pH from 3.0 to 6.0 and concentrations of As(III) and Cr(VI) from 10 to 1000 μM by the photocatalyst material, and the presence of other ion salts such as KCl, Na$_2$SO$_4$ and Mg(NO$_3$)$_2$ had no any inhibitory effect on their conversion. The photogenerated species such as hole coupled with superoxide radical and photogenerated electron coupled with H$_2$O$_2$ were responsible for the oxidation of As(III) and the reduction of Cr(VI), respectively. Besides, the Cr(V)/H$_2$O$_2$ Fenton-like system that was established during the photocatalytic treatment by g-C$_3$N$_4$ based photo-catalyst, had synergistic impact towards the simultaneous conversion of As(III) and Cr(VI), i.e., reduction of Cr(VI) to Cr(V) as well as generation of hydroxyl radicals for As(III) oxidation.

1. Introduction

The species of chromium and arsenic are prevalently found in the ecosystem and play significant role in the cyclic processes of nature. They have been utilized in the industrial manufacturing processes [1] and pose a severe health risk to humankind upon getting into environment. A major source for the contamination of these pollutants is identified as Acid Mine Drainage (AMD) [2], wherein the species mostly exist as As(III) and Cr(VI) together at a level of high concentrations. As known, a trivalent state of arsenic (As(III)) is more toxic and having high percolation nature compared to As(V) [3]. Similarly, Cr(VI) exhibits high solubility and percolating power in acidic environment, while the less toxic Cr(III) is mostly insoluble and can very well be made as immobilized hydroxide complex even in a wide range of pH scale. Hence, the strategy that comprises pre-oxidation of As(III) to As(V) and pre-reduction of Cr(VI) to Cr(III) followed by a simple adsorptive or coprecipitative treatment, is greatly conducive to the task of a complete removal under acidic condition, and can be a sustainable remedy for humankind.

Developing a green and viable technique for the mentioned issue thus becomes of great practical significance. Though, the conversion seems to be thermodynamically feasible ($E°$ (HCr^{VI}O$_4$$^−$/Cr^{3+}) = +1.38 V, $E°$ (H$_2$As^{V}O$_4$$^−$/HAs^{III}O$_2$) = +0.4 V, vs NHE) [1], the rate at which the direct redox conversion takes place between As(III) and Cr(VI) in dilute aqueous solutions is negligibly slow. The indirect simultaneous conversion is possible by introducing a third redox active substance that would serve as oxidant and reductant for As(III) and Cr(VI), respectively. Hydrogen peroxide (H$_2$O$_2$), that could react with both As(III) and Cr(VI) ($E°$ (H$_2$O$_2$/H$_2$O) = +1.77 V vs NHE, $E°$ (O$_2$/H$_2$O$_2$) = +0.68 V, vs NHE), has been proved to be a competent among the active redox substances. For example, the simultaneous redox conversion of As(III) and Cr(VI) was realized by utilizing H$_2$O$_2$ directly [2] and generated from AuPd/CNTs electrocatalysis [4]. In the process, the intermediates of Cr(V) produced by reaction of Cr(VI) with H$_2$O$_2$ play an important role for the oxidization of As(III) to As(V) through hydroxyl radicals (˙OH). Besides, the generation of redox species with photocatalytic material is an alternate option, i.e., photogenerated electron (e$^−$) as reductant for the reduction of Cr(VI) and hole (h$^+$) as oxidant for the oxidation of As(III).

Photocatalytic technology, especially TiO$_2$-based photocatalytic technology has been widely studied and applied for the actual engineering aspect of wastewater treatment [5–12]. However, its wide

---

band gap (~ 3.2 eV) cannot take advantage of the large proportion of visible light in the sunlight and thereby greatly hinders the ability to maximize the solar-to-chemical energy conversion efficiency. For more efficient sunlight application, visible light driven photocatalyst appeals much more interests recently [7,9,13,14]. Among them, graphitic carbon nitride (g-C$_3$N$_4$) stands out as photocatalyst for environmental remediation especially water treatment due to its abundance and cheap precursors, simple synthesis process, and excellent optical absorption in visible light region [15–20]. Moreover, g-C$_3$N$_4$, as a metal-free polymeric photocatalyst with a graphitic stacking structure of melem sheets, showed a selectivity in the photocatalytic production of H$_2$O$_2$ [21]. Although the performance of pristine g-C$_3$N$_4$ in water media is poor, due to a fast intrinsic recombination of the photoexcited carriers and a low valence band (VB) energy level, its photocatalytic activity for H$_2$O$_2$ generation from pure water and O$_2$ gas can be promoted by incorporating electron-deficient or π-conjugated monomers into the lattice network of g-C$_3$N$_4$ [22].

In this study, a composite photocatalyst comprised the g-C$_3$N$_4$ with pyromellitic diimide (PDI) doping was used for the simultaneous photocatalytic redox conversion of Cr(VI) and As(III). The composite catalyst g-C$_3$N$_4$/PDI (gCP) showed a high efficiency and selectivity on photocatalytic generation of H$_2$O$_2$ [22] owing to its enhanced water oxidation capacity [23]. The H$_2$O$_2$ produced in situ was utilized for the synergistic conversion of both the pollutants. The prepared photocatalytic composite material exhibited an effective on treatment of As(III) and Cr(VI), and a satisfactory durability in the recycle photocatalysis run. And as far as we know, there are no reports on the use of g-C$_3$N$_4$ based photocatalyst for simultaneous conversion of the both pollutants so far.

2. Materials and methods

2.1. Materials

Sodium arsenite (NaAsO$_2$), sodium arsenate (Na$_2$HAsO$_4$·7H$_2$O), potassium dichromate (K$_2$Cr$_2$O$_7$), 5,5-dimethyl-pyridine N-oxide (DMPO, 97%) were purchased from Sigma-Aldrich, and H$_2$O$_2$ (30%), KCl, Na$_2$SO$_4$, Mg(NO$_3$)$_2$, NaOH and HCl were purchased from Sinopharm Chemical Reagent (Shanghai, China). All chemical regents were used without further purification. Commercial P25 (TiO$_2$, Degussa) was used as received.

2.2. Preparation and characterization of catalysts

G-C$_3$N$_4$ was prepared by heating 3.0 g melamine at 425 °C for 4 h under N$_2$ flow. The prepared g-C$_3$N$_4$ and PMDA were mixed with three different mass ratio of 1:1 (gCP$_1$), 1:2 (gCP$_2$) and 1:3 (gCP$_3$) by the effective grinding followed by a calcination in corundum crucible at 325 °C for 4 h under N$_2$ flow. The obtained catalyst powders were sufficiently washed with water and vacuum-dried at 60 °C. The detailed experimental procedure was similar to the previous study [22].

The morphological characterization of the prepared catalyst was carried out by using a field emission scanning electron microscopy (FSEM, Sirion 200, FEI) operated at an accelerating voltage of 10 kV. The crystal phase and structure was examined by X-ray diffraction instrument (XRD, Empyrean, PANalytical B.V., Holland) equipped with Cu Kα radiation (40 kV, λ = 1.5406 Å). The chemical structure and composition of the sample were elucidated by using Fourier transforms infrared spectrophotometer (FTIR, VERTEX 70, Bruker, Germany).

The diffuse reflectance spectra (DRS) of the samples were recorded at room temperature with UV–vis spectrophotometer (UV-2600, Shimadzu, Japan). Mott-Schottky plots were performed at different frequencies (1000, 1500, and 2000 Hz) by using electrochemical workstation (CHI760e, CH Instruments, USA) and a 3 mm diameter glassy carbon substrate covered with the samples was employed as working electrode. 10 mg of the catalyst material was mixed with 1 mL

of a solution containing water and alcohol in a ratio of 3:1, and the mixed material was transferred into 40 μL nafion PFSA polymer dispersion (D520 (5%)). The suspension was undergone ultrasonication treatment for 15 min, from which a 10 μL of representative mixture was taken and dripped on the surface of the glassy carbon electrode and the electrode surface was kept in the atmospheric air for drying. The measurements were carried out in a conventional three-electrode cell comprising the prepared catalyst, saturated calomel electrode and platinum gauze as working, reference, and counter electrodes, respectively.

Zeta potential measurements were made with a Zeta Potential Analyzer (ZetaPlus, Brookhaven, USA). The specific surface areas (SSA) and pore volume distribution of the samples were determined by Brunauer Emmett and Teller (BET) N$_2$ adsorption technique at 77 K using a Tristar II surface area and porosity analyser (Micromeritics, USA).

2.3. Experimental procedure

Photocatalytic experiments were carried out in 50 mL aqueous solution in which 50 mg of the catalyst and the target pollutant were added in a container, which was kept in a water jacket cooled by ice to avoid heating of solution under Xenon lamp irradiation and kept the temperature around 20°C. The pH of the suspension was adjusted by adding HCl or NaOH solutions. Prior to every experimental run, ultrasonication treatment was done for a period of 5 min to keep the catalyst suspension completely dispersed and the suspension was stirred in dark for 30 min to facilitate the adsorption-desorption equilibrium between the pollutant and the photocatalysts. A 300 W Xenon lamp (PLS-SXE 300, Perfect light, China) with a cutoff filter of 420 nm was employed as visible light source. During the irradiation treatment, about 1 mL of the representative suspension was taken at a defined time interval, and passed through a 0.45 μm PTFE filter for the chemical analysis. For a recycle experimental run, the suspension employed in the final run was collected and undergone the following treatments. It was filtered, washed thrice with deionized water and dried at 60°C for 6 h period. The dried sample was then employed for a preparative recycle experimental run. Always, an enough quantity of the employed photocatalyst sample was accomplished by repeating the experimental run many times. A sealed stainless steel vessel with a quartz window on the top and two holes as inlet and outlet for gases was used for aeration experiments. The disposal of the residue left behind upon the redox reaction of As(III) and Cr(VI), was carried out as follows. Initially, H$_2$O$_2$ was added to convert As(III) and Cr(VI) into As(V) and Cr(III) and the pH of the residue was adjusted using NaOH to form insoluble Cr(OH)$_3$ species. Subsequently, Fe$_2$(SO$_4$)$_3$ was added to remove initially As(V) followed by Cr(III) further as well by forming the respective insoluble complexes FeAsO$_4$ and Cr$_x$Fe$_{1-x}$(OH)$_3$ [24,25].

2.4. Analytical methods

The speciation of As(III) and As(V) analysis and its quantification was done by using the liquid chromatography (LC-P100, Wufeng, China) equipped with an atomic fluorescence spectrometer (SA-7800, Bohui, China). The total concentration of arsenic was figured out by summing up the concentration of As(III) and As(V). The concentration of Cr(VI) was determined by a modified diphenylcarbazide (DPC) method which is free from the H$_2$O$_2$ interference [26]. The concentrations of total chromium were determined by inductively coupled plasma optical emission spectrometer (ICP, Optima 8300, PerkinElmer, USA). The concentration of Cr(III) was obtained from the difference between total chromium content and Cr(VI). Potassium titanium oxalate method was used to determine the concentration of H$_2$O$_2$ [27]. ·OH was captured by using DMPO as the spin trapper and examined by an electron paramagnetic resonance (EPR; EMXnano, Bruker, Germany) spectral measurement [28].

3. Results and discussion

3.1. Characterization of photocatalysts

The composite photocatalyst of g-C_3N_4/PDI (gCP) was characterized by instrumental analysis such as XRD, FTIR, XPS and UV–vis DRS (Fig. S1–S4), which indicated that the successful formation of PDI units in the composite catalyst and an extended absorption of solar light by the PDI doping. From Mott-Schottky measurements (Fig. S5), the valence band (VB) potential for g-C_3N_4 and three kind of g-C_3N_4/PDI photocatalysts with different mass ratio of 1:1 (gCP$_1$), 1:2 (gCP$_2$) and 1:3 (gCP$_3$) was calculated as $+1.79$ V, $+1.88$ V, $+1.96$ V and $+2.53$ V (vs Ag/AgCl, pH 6.6), respectively, corresponding to conduction band (CB) potential of -1.20 V, -1.07 V, -0.97 V and -0.41 V. Incorporating the π-conjugated monomer of PDI into the lattice network of g-C_3N_4 simultaneously pulled down both the CB and VB positions, and the effect was enhanced with the doping amount of PDI (see Supporting Information).

3.2. Simultaneous oxidation of As(III) and reduction of Cr(VI) by photocatalyst

As shown in Fig. 1(a), the direct redox conversion between As(III) and Cr(VI) was hardly achieved, whereas the removal of Cr(VI) and the accompanied production of As(V) were initiated by the photocatalytic reaction of either g-C_3N_4 or gCP. All three composite photocatalysts of gCP showed more efficient compared to g-C_3N_4, in which gCP$_2$ was the most outstanding photocatalyst (Fig. S6). Moreover, a synergistic effect on the coconversion of As(III) and Cr(VI) was achieved with the gCP$_2$ as shown in Fig. 1(b). The redox rate of As(III) and Cr(VI) in their coexisting system were faster than that in any single system of As(III) or Cr(VI).

The reaction kinetics of redox conversion of As(III) and Cr(VI) could fit well with the pseudo-first order kinetic equation. As shown in Fig. S7, the rate of As(III) oxidation in coexisting system was more facile than that in single As(III) system, they were 0.037 min^{-1} and 0.026 min^{-1}, respectively. Similarly, the rate of Cr(VI) reduction were 0.027 min^{-1} and 0.021 min^{-1}, against the coexisting and single Cr(VI) system, respectively.

TiO$_2$ (P25), a pioneer of the photocatalytic materials, has been extensively used for the preoxidation and prereduction of As(III) and Cr(VI), and hence a comparative study was inevitable [8,29]. As shown in Fig. 2(c–d) and Fig. S8(c–d), the P25 photocatalyst exhibited a good adsorption behavior compared to gCP$_2$. The adsorption of As(III) and Cr(VI) by P25 were 75% and 50% within 30 min, respectively, whereas it was insignificant by using gCP$_2$ within the same duration. On a whole, the performance of P25 on As(III) removal was superior in the first cycle and a complete removal was achieved within 50 min. In the case of Cr(VI) removal, in spite of its strong pre-adsorption, the P25 was little inferior to the performance of gCP$_2$. However, in the recycling experiment of the photocatalyst materials, compared to a stable conversion of the both pollutants by the gCP$_2$, it was drastically fallen by P25. In particular, the removal of Cr(VI) was less than 60% in the fourth

recycle run. Additionally, by the gCP$_2$, the conversion of As(III) got slightly fast with the recycle runs.

3.3. Adsorptive characteristics of photocatalysts

BET surface area analysis was carried out on gCP$_2$ and P25 powder materials to compare their adsorption capacity. As listed in Table 1, it was found that the P25 sample had over 12 times higher surface area and larger pore volumes than the gCP$_2$ powder, providing the P25 sample with excellent adsorption capacity. Measurements of Zeta-potential indicated a more negative zeta potentials with an increase in pH value for both the samples. However, the gCP$_2$ showed a negative charge, while the P25 exhibited a positive charge in the pH range between 3.0 and 6.0 (Fig. 3). The results suggested that the P25 sample inherently had strong adsorptive nature to accommodate the anions such as AsO$_2^-$ and HCrO$_4^-$ [4], as well as the oxidative production of As(III) viz. H$_2$AsO$_4^-$ [30] in the pH range while the gCP$_2$ did not. Specially, the formation of bidentate binuclear surface complex for both As(V) and As(III) with an average bond distance of 3.30 Å (Ti-As(V)) and 3.35 Å (Ti-As(III)) was evidenced on the TiO$_2$-based photocatalyst [31]. The adsorption of product species would cover up the active sites of the photocatalyst thereby a deactivation of the photocatalyst is inevitable [8]. The poor durability of P25 photocatalyst is being the key technical bottleneck for its practical application.

Non adsorptive nature of gCP$_2$ towards the products, especially As(III) oxidation product might be a cause for its stable performance on simultaneous redox conversion of As(III) and Cr(VI). To further ascertain the interpretation, XPS analysis was carried out for the material that underwent four recycle runs.

As shown in Fig. 4 and Fig. S8(a–b), the As 3d XPS spectra of the employed catalyst in the binding energy range of 36–48 eV [29] was insignificant, which indicated that very trace concentration of As species was remained on the catalyst, while the Cr 2p spectra exhibited less prominent peak that reflected the Cr(III) species [32,33]. From the mass balance calculation between total Cr and only Cr(VI) during the reaction, the amount of Cr(III) remained on the catalyst surface after reactions was confirmed to be very little. Together with the in-situ generated H$_2$O$_2$ by g-C_3N_4 based photocatalysis, Fenton-like system of Cr(III)/H$_2$O$_2$ would be established to produce hydroxyl radical [34], which in fact makes the conversion of As(III) gradually increased from 0.037 min^{-1} to 0.041 min^{-1}, 0.044 min^{-1} and 0.046 min^{-1} in the four recycle runs (Fig. 2).

3.4. Effects of PDI amount

The amount of PDI units strongly affects the catalytic activity. As shown in Fig. S6, compared with g-C_3N_4, three kind of g-C_3N_4/PDI photocatalysts, viz. gCP$_1$, gCP$_2$ and gCP$_3$ showed the higher photocatalytic performances for the simultaneous redox removal of As(III) and Cr(VI). Furthermore, the simultaneous removal was positively related to the production of H$_2$O$_2$ in pure water and coexisting As(III) and Cr(VI) solutions (Fig. S9). The catalyst prepared with 1:2 mass ratio (gCP$_2$) exhibited the highest activity in terms of H$_2$O$_2$ generation as
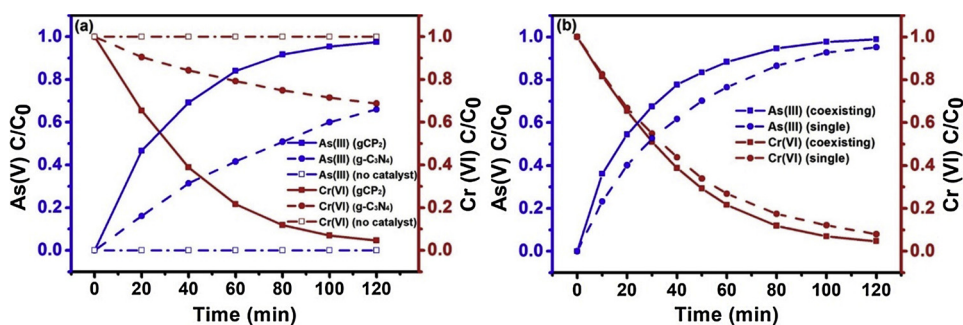

Fig. 1. (a) Simultaneous redox conversion performance of Cr(VI) and As(III) in presence of gCP$_2$ or g-C_3N_4 under visible-light irradiation (λ > 420 nm), and direct conversion without the photocatalyst. (b) Comparison of simultaneous redox conversion of As(III) and Cr(VI) in coexisting system and their solo conversion in single system with the gCP$_2$ photocatalysis. Experimental conditions (the same as other Figs. unless otherwise stated): [cat.] = 1.0 g/L, [As(III)]$_0$ = 100 μM, [Cr(VI)]$_0$ = 100 μM, pH = 4, and λ > 420 nm.
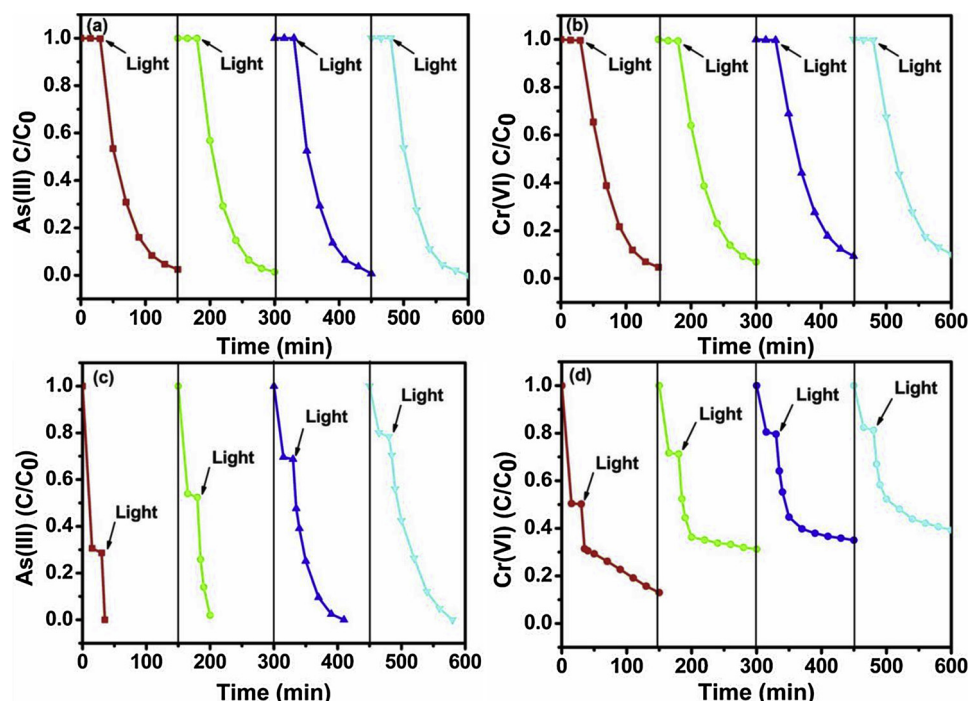
Fig. 2. Recycle performance of simultaneous redox conversion of As(III) and Cr(VI) in coexisting system by photocatalysis with gCP$_2$ (a, b) and P25 (c, d).

Table 1
Texture properties of gCP$_2$ and P25 samples.

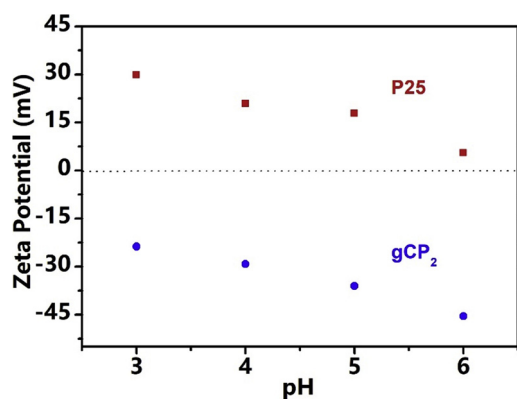| Samples	BET surface area (m^2/g)	Volume of pores (cm^3/g)
gCP$_2$	3.4	0.004
P25	43.5	0.066

Fig. 3. Zeta potentials of gCP$_2$ and P25 samples.

well as on the simultaneous redox conversion of As(III) and Cr(VI).

3.5. Effects of initial pH, concentration of As(III) and Cr(VI), and ion salts

As seen in Fig. S10, the initial pH of 3.0, 4.0, 5.0 and 6.0 was found to have impact on the simultaneous redox conversion of the pollutants As(III) and Cr(VI), especially for the reduction of Cr(VI). The reduction conversion of Cr(VI) was 30.1%, 39.4% and 61.1% upon 50 min irradiation at the initial pH 6.0, 5.0 and 4.0, respectively, and increased to 100% at the initial pH of 3.0. The synergistic effect was invariably found with the different initial pH, and highly pronounced at pH 4.0 (Table S1). Thus, the photocatalytic experiments were carried out at pH 4.0 for elucidating the reaction mechanism.

The rate of conversion of As(III) and Cr(VI) was decreased with an increase in their initial concentration. Though, the rate of As(III) and Cr (VI) conversion fell significantly down from 0.091 min^{-1}, 0.037 min^{-1} to 0.007 min^{-1}, and 0.041 min^{-1}, 0.027 min^{-1} to 0.004 min^{-1} respectively as the concentration of the pollutants increased from 10 μM, 100 μM to 1000 μM, the quantity of conversion obtained from the last one system upon 120 min period was as large as 560 μM and 378 μM against As(III) and Cr(VI) respectively (Fig. S11).

The effect of ion salts on the simultaneous redox conversion of As (III) and Cr(VI) was investigated. Inorganic salt such as KCl, Na$_2$SO$_4$, Mg(NO$_3$)$_2$ at 0.1 M was respectively added into the photocatalytic reaction system. As displayed in Fig. 5, no any inhibitory effect on the redox conversion of As(III) and Cr(VI) by gCP$_2$ was observed with their coexistence in the system. Irrespective of these cations (K$^+$, Na$^+$ and Mg^{2+}) and anions (Cl$^-$, SO$_4^{2-}$ and NO$_3^-$) existed, the As(III) and Cr (VI) could be completely conversed in 120 min. Non-adsorptive dependent removal of As(III) and Cr(VI) by gCP should contribute to the effect, which was contrast to that by TiO$_2$ based photocatalyst. The coexistence of anions was found to be detrimental to the conversion of the both pollutants due to their competitive adsorption on the TiO$_2$ based catalyst [35,36].

3.6. Mechanism: contribution of active species

The photogenerated e$^-$ and h$^+$ were responsible for the reduction of Cr(VI) and the oxidation of As(III), respectively. Also, the photoelectron could reduce the dissolved O$_2$ that coexisted in aqueous solution into superoxide radical ($\cdot$O$_2^-$) or H$_2$O$_2$ via one- or two- electron reduction steps (Eqs. (1) and (2)). As shown in Fig. 6, As(III) oxidization was drastically decreased with the addition of BQ, indicating that the main active specie was $\cdot$O$_2^-$. In O$_2$-aerated solution (Fig. S12), the rate of As(III) oxidation was accelerated significantly, which could be ascribed to the abundance generated $\cdot$O$_2^-$. Besides from the reduction of the dissolved O$_2$, $\cdot$O$_2^-$ could also be formed by the oxidation of As(III) into As(IV) (Eq. (3)), and then the oxidation of As (IV) to As (V) via O$_2$ (Eq. (4)) [6].

$$O_2 + e- \rightarrow \cdot O_2- \tag{1}$$

$$O_2 + 2e- + 2H^+ \rightarrow H_2O_2 \tag{2}$$
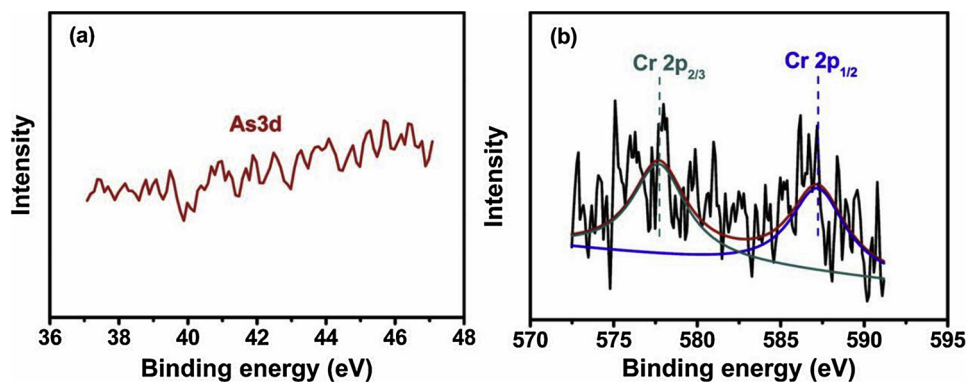
Fig. 4. As 3d (a) and Cr 2p (b) peaks in XPS spectra of gCP$_2$ after four cycles photocatalysis.
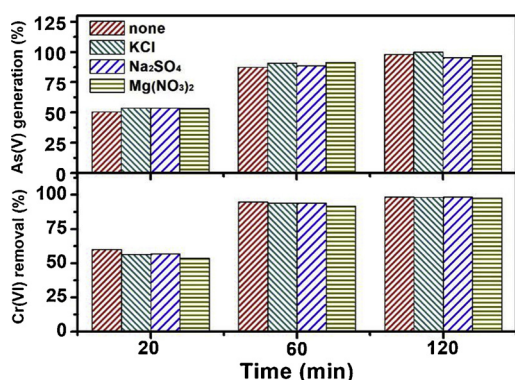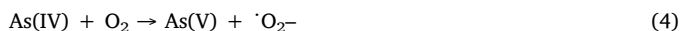

Fig. 5. Comparison of redox conversion of As(III) and Cr(VI) without and with the presence of 0.1 M KCl, Na$_2$SO$_4$ and Mg(NO$_3$)$_2$ respectively in coexisting system.

$$As(III) + \cdot O_2- + 2H^+ \rightarrow As(IV) + H_2O_2 \qquad (3)$$

$$As(IV) + O_2 \rightarrow As(V) + \cdot O_2- \qquad (4)$$

Under N$_2$ atmosphere, the oxidation of As (III) into As(V) decreased from 100% to 67.1% after 80 min (Fig. S12), which should be mainly originated from the contribution of h$^+$. The As (III) could be oxidized into As(V) with the gCP$_2$ due to its more positive VB potential (+2.19 V vs NHE) than the oxidization of As(III) ($E°$(H$_2$As^{V}O$_4^-$/HAs^{III}O$_2$) = +0.4 V vs NHE). However, the actual contribution of h$^+$ must be less than 67.1% taking into account of the dissolved oxygen that could never be eliminated completely. Under an ambient atmosphere, the oxidation of As(III) was decreased by ˜11.7% with the addition of EDTA (Fig. 6(a)), which is a well-known h$^+$ scavenger. Since the EDTA not only scavenges the h$^+$, but also reduces the recombination of e$^-$ and

h$^+$, more ˙O$_2^-$ was formed by reduction of O$_2$ on CB with more active photoelectron production due to h$^+$ quenching. The oxidation of As(III) by the ˙O$_2^-$ would then be enhanced, i.e., the actual oxidation of As(III) by h$^+$ (Eqs. (5) and (6)) must be a higher than the value that showed in Fig. 6(a). Conclusively, the efficiency of oxidation of As(III) by h$^+$ could be in between 11.7% and 67.1%.

The alternative active species for the oxidation of As(III) was probably ˙OH, which could be produced from the oxidation of H$_2$O by the h$^+$ in the photocatalytic system. However, no proven pathway for the oxidation via the ˙OH in the single As(III) photocatalytic system was established (Eqs. (7) and (8)), which was confirmed by quenching of the radical with an addition of TBA (Fig. 6(a)), and by the weak DMPO-˙OH signal of ESR as well (Fig. 7(a)). The photocatalytic generation of ˙OH by the gCP$_2$ was insignificantly, as it has lower and insufficient VB energy level (+2.19 V vs NHE) to yield ˙OH from oxidation of H$_2$O ($E°$ (˙OH/H$_2$O) = +2.7 V vs NHE) [37]. In contrast, in the As(III) and Cr (VI) coexisting system, the generation of ˙OH and its role on oxidation of As(III) to As(V) were confirmed by the concrete evidences observed from both ˙OH quenching test and DMPO-˙OH spin adduct characteristic peak (Fig. 6(b) and Fig. 7(a)). Previous studies [2,4] showed that Cr(VI) could be converted into Cr(V) and the ˙OH could be generated from Cr(V)/H$_2$O$_2$ Fenton-like reaction system in presence of H$_2$O$_2$. The pre-requirement for establishing the Cr(V)/H$_2$O$_2$ Fenton-like reaction system, is the generation of Cr(V), which was detected by UV absorption spectra and confirmed by the peak observed > 500 nm that raised up as the gCP$_2$ photocatalytic treatment progressively proceeded (Fig. 7(b)).

$$As(III) + h^+ \rightarrow As(IV) \qquad (5)$$

$$As(IV) + h^+ \rightarrow As(V) \qquad (6)$$

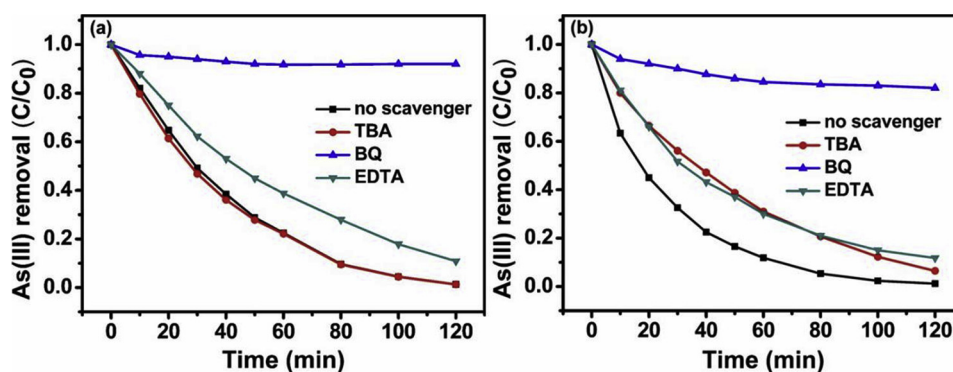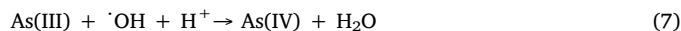$$As(III) + \cdot OH + H^+ \rightarrow As(IV) + H_2O \qquad (7)$$

Fig. 6. Photocatalytic oxidation of As(III) in single system (a) and simultaneous redox conversion of As(III) and Cr(VI) in coexisting system (b) with the gCP$_2$ photocatalysis in the presence of TBA, BQ and EDTA.
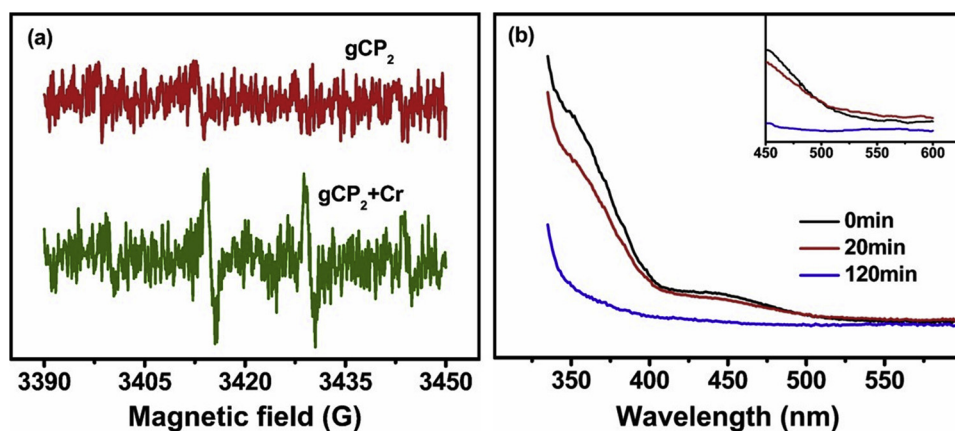
Fig. 7. (a) Hyperfine EPR spectra of the DMPO-$\cdot$OH without (red line) and with Cr(VI) (green line) in the gCP$_2$ photocatalytic system. (b)Variation of UV–vis absorption spectra of Cr (V) in the process of gCP$_2$ photocatalysis in coexisting system (For interpretation of the references to colour in this figure legend, the reader is referred to the web version of this article).
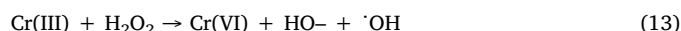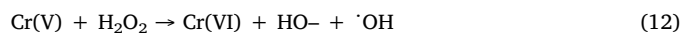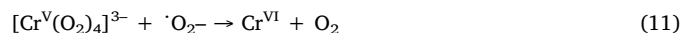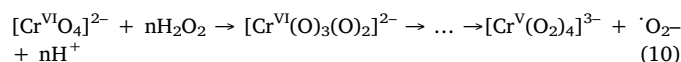
$$As(IV) + \cdot OH + H^+ \rightarrow As(V) + H_2O \tag{8}$$

$$As(IV) + \cdot O_2- + 2H^+ \rightarrow As(V) + H_2O_2 \tag{9}$$
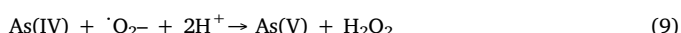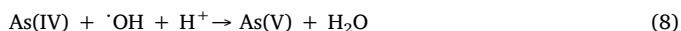
Because $\cdot O_2^-$ was the main active specie for the As(III) oxidation, and the enhancement of the oxidation observed with the addition of Cr (VI) further confirmed the synergistic impact on oxidation of As(III) by H$_2$O$_2$ in presence of Cr(VI) as shown in Fig. 1(b). Otherwise, the enhancement would have not been found due to less reduction of O$_2$ to form $\cdot O_2^-$ caused by competition between O$_2$ and Cr(VI) to react with the e$^-$ of CB.

3.7. Mechanism: contribution of H$_2$O$_2$

With the single As(III) presented, the H$_2$O$_2$ production was hiked in the gCP$_2$ photocatalysis system as shown in Fig. 8(a). The active species such as $\cdot O_2^-$ and h$^+$ were contributed to the oxidation of As(III) in the absence of Cr(VI), as described above. Furthermore, the oxidization of As(III) by $\cdot O_2^-$ would generate an equivalent quantity of H$_2$O$_2$ in Cr (VI) free system (Eqs. (3) and (9)), viz. the presence of single As(III) had no any impact on the amount of H$_2$O$_2$ produced from $\cdot O_2^-$ reduction by photocatalyst. On the other hand, the oxidation of As(III) by h$^+$ would facilitate the seperation of photogenerated h$^+$ with e$^-$ which promoted the quantity of available e$^-$, and would increase the H$_2$O$_2$ production (Eqs. (2)–(6) and (9)). The process of producing 1 mol of H$_2$O$_2$ from O$_2$ reduction requires 2 mol of electron (Eq. (2)), which is equal to the released electron from the oxidation of As(III) to As(V). The trend from the differential of H$_2$O$_2$ production (Fig. 8(b) (m–n)) between the presence and the absence of As(III) was surly showing high degree of consistency with the performance of As(V) generation (Fig. 8(b)). That is, the electrons of 200 μM required for the excess production of H$_2$O$_2$ to an extent of 100 μM (Fig. 8(b) (m–n)) in the 100 μM As(III) presented system, exactly matched with the figure of electrons input onto the VB of photocatalyst and $\cdot O_2^-$ by the oxidation of 100 μM As(III) into As(V). The oxidation of As(III) at a cost of h$^+$ that generated from VB, could effectively separate the photogenerated electrons of CB, and at a

conversion of $\cdot O_2^-$ to H$_2$O$_2$, which together caused the increased production of H$_2$O$_2$.

On the contrary, in the presence of Cr(VI), the production of H$_2$O$_2$ was declined in the gCP$_2$ photocatalysis system as shown in Fig. 8(a). The observed decline could be originated from two ways: (1) competitive reduction reaction of Cr(VI) with that of O$_2$; and (2) the generated H$_2$O$_2$ consumed by reacting with [Cr^{VI}O$_4$]$^{2-}$ or the adsorbed Cr(III) on the catalyst. The reduction of [Cr^{VI}O$_4$]$^{2-}$ by the in-situ photogenerated H$_2$O$_2$ led to the formation of [Cr^V(O$_2$)$_4$]$^{3-}$, and it could be oxidized back by $\cdot O_2-$ (Eqs. (10) and (11)). Otherwise, it would establish the Cr(V)/ H$_2$O$_2$ or Cr(III)/H$_2$O$_2$ Fenton-like reaction system to generate active $\cdot OH$ (Eq. (12) and (13)). In every case, the final product of the reaction was Cr(VI).

$$[Cr^{VI}O_4]^{2-} + nH_2O_2 \rightarrow [Cr^{VI}(O)_3(O_2)]^{2-} \rightarrow \ldots \rightarrow [Cr^V(O_2)_4]^{3-} + \cdot O_2- + nH^+ \tag{10}$$

$$[Cr^V(O_2)_4]^{3-} + \cdot O_2- \rightarrow Cr^{VI} + O_2 \tag{11}$$

$$Cr(V) + H_2O_2 \rightarrow Cr(VI) + HO- + \cdot OH \tag{12}$$

$$Cr(III) + H_2O_2 \rightarrow Cr(VI) + HO- + \cdot OH \tag{13}$$

Over 90% of Cr(VI) conversion obtained within 120 min irrespective of the As(III) addition, suggested that the promoted e$^-$ by the oxidation of As(III) to As(V) had little effect on the reduction of Cr(VI). To find out the fate of the electron that involved in As(III) and Cr(VI) coexisting system, the difference curve (j − i) of H$_2$O$_2$ generation between the coexisting system (j) and the single Cr(VI) system (i) was deduced. Both of two difference curves represented the difference in the presence and absence of As(III) overall, but the curve (j − i) was obviously far lower than the curve (m − n) (Fig. 8(b)). In the case of Cr(VI) coexisting system, the instant production of Cr(V) and the adsorbed Cr(III) with the in-situ generation of H$_2$O$_2$ would form a Fenton-like system that yielded $\cdot OH$ (Eq. (12)), along with a re-conversion of Cr(V) into Cr(VI). The generated $\cdot OH$ reacted with either As(III) or As(IV) (Eqs. (7) and (8)) and accepted an electron which yielded H$_2$O instead of H$_2$O$_2$.
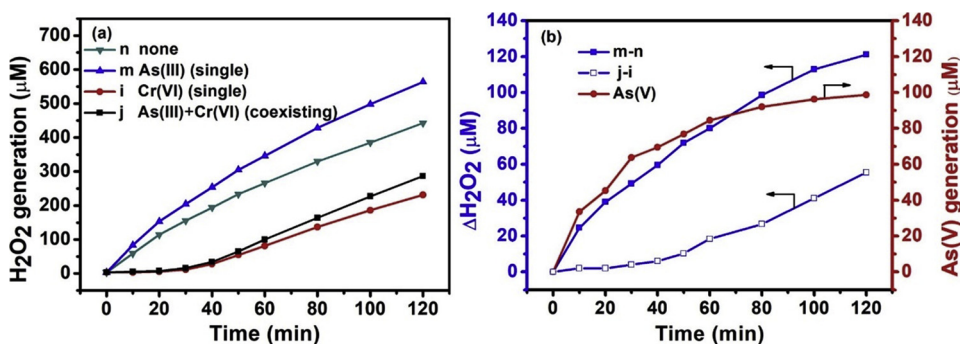

Fig. 8. (a) Generation of H$_2$O$_2$ in the process of gCP$_2$ photocatalysis in different systems. (b) H$_2$O$_2$ molar concentration differences observed between the two single systems viz. simple aqueous and presence of As(III) alone (m–n), and between the coexisting As(III) and Cr(VI) system and the single Cr(VI) system (j-i); generation of As(V) from single As(III) system.

Consequently, the oxidation of As(III) by photogenerated h^+ could promote the reduction of Cr(VI) via efficient separation of e–h^+, however, the reformed Cr(VI) by the Cr(V)/H_2O_2 Fenton-like reaction balanced the promotion. On the other hand, the ·OH generated by the Fenton-like reaction could effectively oxidize the As(III) into As(V).

4. Conclusions

In this study, the composite photocatalyst of gCP was found to be superior on synergetic redox conversion of As(III) and Cr(VI) under visible-light irradiation in acidic media. Compared to TiO_2 (P25) based photocatalysis, gCP showed excellent durability because of the non-adsorptive nature towards oxidation product As(V). Furthermore, a small adsorption of cation of reduction product Cr(III) on the gCP surface promoted the oxidation of As(III). On the other hand, the efficiency of simultaneous redox removal of As(III) and Cr(VI) was dependent on the quantity of H_2O_2 produced by the composite photocatalysts. Specifically, the gCP_2 with a composition of 1:2 g-C_3N_4/PDI was highly effective on H_2O_2 production, consequently the most efficient for the simultaneous redox conversion of As(III) and Cr(VI). Besides photocatalytic active species such as e–h^+, ·O_2^- and H_2O_2, the ·OH formed from the in-situ established Cr(V)/H_2O_2 Fenton-like system was confirmed to be contributed to the simultaneous redox conversion of the both pollutants. Meanwhile, the oxidation of As(III) in the photocatalytic process enhanced the production of H_2O_2, that caused promotion of Cr(V)/H_2O_2 Fenton-like system effect. The excellent capacity obtained in the redox conversion, no any inhibitory effect by the co-existed salt ions and the stability of the photocatalyst during the recycle experimental runs along with a synergistic impact confirmed the suitability of gCP_2 photocatalyst for the simultaneous redox removal of As(III) and Cr(VI) in acidic water.

Appendix A. Supplementary data

Supplementary material related to this article can be found, in the online version, at doi:https://doi.org/10.1016/j.apcatb.2019.02.041.

References

[1] K. Kim, W. Choi, Enhanced redox conversion of chromate and arsenite in ice, Environ. Sci. Technol. 45 (2011) 2202–2208, https://doi.org/10.1021/es103513u.
[2] Z. Wang, R.T. Bush, L.A. Sullivan, J. Liu, Simultaneous redox conversion of chromium(VI) and arsenic(III) under acidic conditions, Environ. Sci. Technol. 47 (2013) 6486–6492, https://doi.org/10.1021/es400547p.
[3] V. Vaiano, G. Iervolino, D. Sannino, L. Rizzo, G. Sarno, A. Farina, Enhanced photocatalytic oxidation of arsenite to arsenate in water solutions by a new catalyst based on MoO_x supported on TiO_2, Appl. Catal. B Environ. 160–161 (2014) 247–253, https://doi.org/10.1016/j.apcatb.2014.05.034.
[4] M. Sun, G. Zhang, Y. Qin, M. Cao, Y. Liu, J. Li, J. Qu, H. Liu, Redox conversion of chromium(VI) and arsenic(III) with the intermediates of chromium(V) and arsenic (IV) via AuPd/CNT_s electrocatalysis in acid aqueous solution, Environ. Sci. Technol. 49 (2015) 9289–9297, https://doi.org/10.1021/acs.est.5b01759.
[5] M.N. Chong, B. Jin, C.W.K. Chow, C. Saint, Recent developments in photocatalytic water treatment technology: a review, Water Res. 44 (2010) 2997–3027, https://doi.org/10.1016/j.watres.2010.02.039.
[6] H. Lee, W. Choi, Photocatalytic oxidation of arsenite in TiO_2 suspension: kinetics and mechanisms, Environ. Sci. Technol. 36 (2002) 3872–3878, https://doi.org/10.1021/es0158197.
[7] G. Li, X. Nie, J. Chen, Q. Jiang, T. An, P.K. Wong, H. Zhang, H. Zhao, H. Yamashita, Enhanced visible-light-driven photocatalytic inactivation of *Escherichia coli* using g-C_3N_4/TiO_2 hybrid photocatalyst synthesized using a hydrothermal-calcination approach, Water Res. 86 (2015) 17–24, https://doi.org/10.1016/j.watres.2015.05.053.

[8] Y. Li, Y. Bian, H. Qin, Y. Zhang, Z. Bian, Photocatalytic reduction behavior of hexavalent chromium onhydroxyl modified titanium dioxide, Appl. Catal. B Environ. 206 (2017) 293–299, https://doi.org/10.1016/j.apcatb.2017.01.044.
[9] T. Ochiai, K. Nakata, T. Murakami, A. Fujishima, Y. Yao, D.A. Tryk, Y. Kubota, Development of solar-driven electrochemical and photocatalytic water treatment system using a boron-doped diamond electrode and TiO_2 photocatalyst, Water Res. 44 (2010) 904–910, https://doi.org/10.1016/j.watres.2009.09.060.
[10] M.P. Reddy, A. Venugopal, M. Subrahmanyam, Hydroxyapatite-supported Ag–TiO_2 as *Escherichia coli* disinfection photocatalyst, Water Res. 41 (2007) 379–386, https://doi.org/10.1016/j.watres.2006.09.018.
[11] L. Rizzo, A. Della Sala, A. Fiorentino, G.L. Puma, Disinfection of urban wastewater by solar driven and UV lamp–TiO_2 photocatalysis: effect on a multi drug resistant *Escherichia coli* strain, Water Res. 53 (2014) 145–152, https://doi.org/10.1016/j.watres.2014.01.020.
[12] Z. Xiong, J. Ma, W.J. Ng, T.D. Waite, X.S. Zhao, Silver-modified mesoporous TiO_2 photocatalyst for water purification, Water Res. 45 (2011) 2095–2103, https://doi.org/10.1016/j.watres.2010.12.019.
[13] C. Xue, T. Zhang, S. Ding, J. Wei, G. Yang, Anchoring tailored low-index faceted BiOBr nanoplates onto TiO_2 nanorods to enhance the stability and visible-light-driven catalytic activity, ACS Appl. Mater. Interfaces 9 (2017) 16091–16102, https://doi.org/10.1021/acsami.7b00433.
[14] X. Bai, Y. Du, X. Hu, Y. He, C. He, E. Liu, J. Fan, Synergy removal of Cr (VI) and organic pollutants over RP-MoS_2/rGO photocatalyst, Appl. Catal. B Environ. 239 (2018) 204–213, https://doi.org/10.1016/j.apcatb.2018.08.016.
[15] F. Dong, L. Wu, Y. Sun, M. Fu, Z. Wu, S.C. Lee, Efficient synthesis of polymeric g-C_3N_4 layered materials as novel efficient visible light driven photocatalysts, J. Mater. Chem. 21 (2011) 15171–15174, https://doi.org/10.1039/C1JM12844B.
[16] Y. Li, C. Zhang, D. Shuai, S. Naraginti, D. Wang, W. Zhang, Visible-light-driven photocatalytic inactivation of MS2 by metal-free g-C_3N_4: virucidal performance and mechanism, Water Res. 106 (2016) 249–258, https://doi.org/10.1016/j.watres.2016.10.009.
[17] W. Liao, M. Murugananthan, Y. Zhang, Synthesis of Z-scheme g-C_3N_4–Ti^{3+}/TiO_2 material: an efficient visible light photoelectrocatalyst for degradation of phenol, Phys. Chem. Chem. Phys. 17 (2015) 8877–8884, https://doi.org/10.1039/C5CP00639B.
[18] B. Lin, H. Li, H. An, W. Hao, J. Wei, Y. Dai, C. Ma, G. Yang, Preparation of 2D/2D g-C_3N_4 nanosheet@$ZnIn_2S_4$ nanoleaf heterojunctions with well-designed high-speed charge transfer nanochannels towards highefficiency photocatalytic hydrogen evolution, Appl. Catal. B Environ. 220 (2018) 542–552, https://doi.org/10.1016/j.apcatb.2017.08.071.
[19] B. Lin, H. An, X. Yan, T. Zhang, J. Wei, G. Yang, Fish-scale structured g-C_3N_4 nanosheet with unusual spatial electrontransfer property for high-efficiency photocatalytic hydrogenevolution, Appl. Catal. B Environ. 210 (2017) 173–183, https://doi.org/10.1016/j.apcatb.2017.03.066.
[20] B. Lin, J. Li, B. Xu, X. Yan, B. Yang, J. Wei, G. Yang, Spatial positioning effect of dual cocatalysts accelerating charge transfer in three dimensionally ordered macroporous g-C_3N_4 for photocatalytic hydrogen evolution, Appl. Catal. B Environ. 243 (2019) 94–105, https://doi.org/10.1016/j.apcatb.2018.10.029.
[21] D. Masih, Y. Ma, S. Rohani, Graphitic C_3N_4 based noble-metal-free photocatalyst systems: a review, Appl. Catal. B Environ. 206 (2017) 556–588, https://doi.org/10.1016/j.apcatb.2017.01.061.
[22] Y. Shiraishi, S. Kanazawa, Y. Kofuji, H. Sakamoto, S. Ichikawa, S. Tanaka, T. Hirai, Sunlight-driven hydrogen peroxide production from water and molecular oxygen by metal-free photocatalysts, Angew. Chem. Int. Ed. 53 (2014) 13454–13459, https://doi.org/10.1002/anie.201407938.
[23] Y. Kofuji, Y. Isobe, Y. Shiraishi, H. Sakamoto, S. Tanaka, S. Ichikawa, T. Hirai, Carbon nitride-aromatic diimide-graphene nanohybrids: metal-free photocatalysts for solar-to-hydrogen peroxide energy conversion with 0.2% efficiency, J. Am. Chem. Soc. 138 (2016) 10019–10025, https://doi.org/10.1021/jacs.6b05806.
[24] W. Liu, L. Jin, J. Xu, J. Liu, Y. Li, P. Zhou, C. Wang, R.A. Dahlgren, X. Wang, Insight into pH dependent Cr(VI) removal with magnetic Fe_3S_4, Chem. Eng. J. 359 (2019) 564–571.
[25] E.O. Kartinen Jr., C.J. Martin, An overview of arsenic removal processes, Desalination 103 (1995) 79–88.
[26] A.D. Bokare, W. Choi, Advanced oxidation process based on the Cr(III)/Cr(VI) redox cycle, Environ. Sci. Technol. 45 (2011) 9332–9338, https://doi.org/10.1021/es2021704.
[27] R.M. Sellers, Spectrophotometric determination of hydrogen peroxide using potassium titanium(IV) oxalate, Analysis 105 (1980) 950–954, https://doi.org/10.1039/AN9800500950.
[28] Z. Zhu, H. Pan, M. Murugananthan, J. Gong, Y. Zhang, Visible light-driven photocatalytically active g-C_3N_4 material for enhanced generation of H_2O_2, Appl. Catal. B Environ. 232 (2018) 19–25, https://doi.org/10.1016/j.apcatb.2018.03.035.
[29] J. Kim, J. Kim, Arsenite oxidation-enhanced photocatalytic degradation of phenolic pollutants on platinized TiO_2, Environ. Sci. Technol. 48 (2014) 13384–13391, https://doi.org/10.1021/es504082r.
[30] P.L. Smedley, D.G. Kinniburgh, A review of the source, behaviour and distribution of arsenic in natural waters, Appl. Geochem. 17 (2002) 517–568, https://doi.org/10.1016/S0883-2927(02)00018-5.
[31] X. Guan, J. Du, X. Meng, Y. Sun, B. Sun, Q. Hu, Application of titanium dioxide in arsenic removal from water: a review, J. Hazard. Mater. 215–216 (2012) 1–16, https://doi.org/10.1016/j.jhazmat.2012.02.069.
[32] M.C. Biesinger, C. Brown, J.R. Mycroft, R.D. Davidson, N.S. McIntyre, X-ray photoelectron spectroscopy studies of chromium compounds, Surf. Interface Anal. 36 (2004) 1550–1563, https://doi.org/10.1002/sia.1983.
[33] E. Ünveren, E. Kemnitz, S. Hutton, A. Lippitz, W.E.S. Unger, Analysis of highly

resolved x-ray photoelectron Cr 2p spectra obtained with a Cr_2O_3 powder sample prepared with adhesive tape, Surf. Interface Anal. 36 (2004) 92–95, https://doi.org/10.1002/sia.1655.

[34] A.D. Bokare, W. Choi, Review of iron-free Fenton-like systems for activating H_2O_2 in advanced oxidation processes, J. Hazard. Mater. 275 (2014) 121–135, https://doi.org/10.1016/j.jhazmat.2014.04.054.

[35] D.S. Bhatkhande, V.G. Pangarkar, A. Beenackers, Photocatalytic degradation for environmental applications – a review, J. Chem. Technol. Biot. 77 (2002) 102–116, https://doi.org/10.1002/jctb.532.

[36] S. Sontakke, J. Modak, G. Madras, Effect of inorganic ions, H_2O_2 and pH on the photocatalytic inactivation of *Escherichia coli* with silver impregnated combustion synthesized TiO_2 catalyst, Appl. Catal. B Environ. 106 (2011) 453–459, https://doi.org/10.1016/j.apcatb.2011.06.003.

[37] G.-h. Moon, S. Kim, Y.-J. Cho, J. Lim, D.-h. Kim, W. Choi, Synergistic combination of bandgap-modified carbon nitride and WO_3 for visible light-induced oxidation of arsenite accelerated by in-situ Fenton reaction, Appl. Catal. B Environ. 218 (2017) 819–824, https://doi.org/10.1016/j.apcatb.2017.07.021.